

Supplementary Information for

Nanoscale Insight into the Degradation Mechanisms of the Cartilage Articulating Surface Preceding OA

Tooba Shoaib^{a&}, Catherine Yuh^{b&}, Markus A. Wimmer^{b*}, Thomas Schmid^b, and Rosa M. Espinosa-Marzal^{a,c*}

a. Materials Science and Engineering, University of Illinois at Urbana-Champaign, 1304 W Green St, Urbana, Illinois 61801, United States.

b. Department of Orthopedics, Rush University Medical Center, Chicago, IL.

c. Civil and Environmental Engineering Department, University of Illinois at Urbana-Champaign, Urbana, IL.

*Corresponding author.

&Contributed equally

Rosa M. Espinosa-Marzal, Tel: +1 217 607 3856, E-mail address: rosae@illinois.edu

Markus A. Wimmer, Tel: +1 312 942 2789, E-mail address: Markus_A_Wimmer@rush.edu

This PDF file includes:

Figs. S1 to S6

Tables S1 to S3

References for SI reference citations

Reference SFA experiments

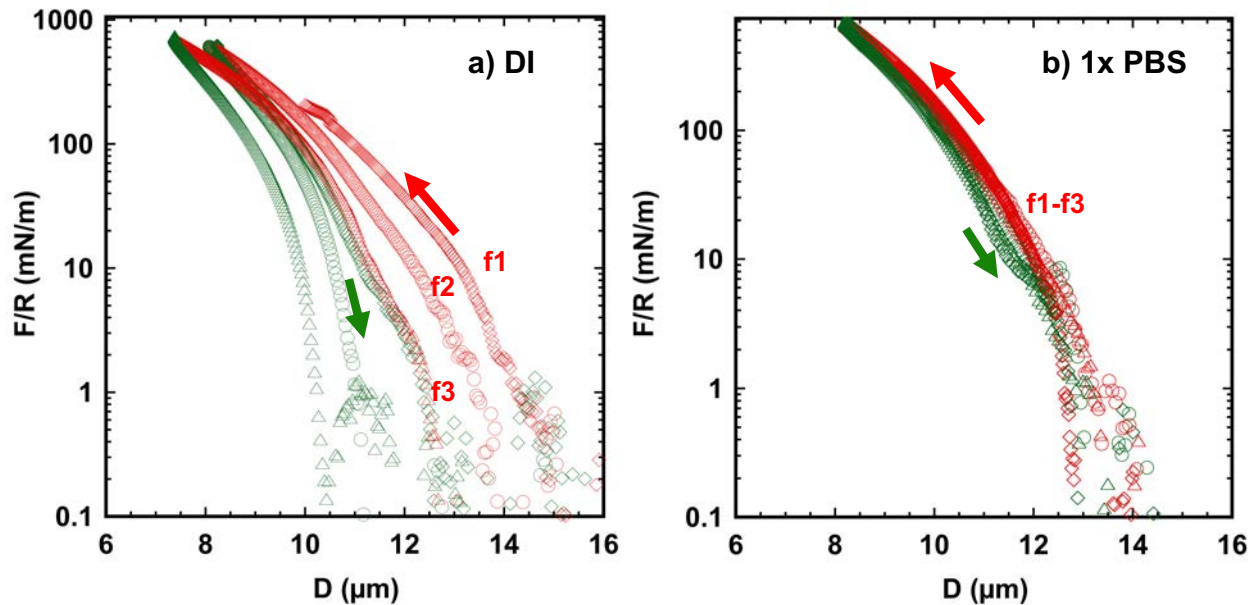


Figure S1. Reference eSFA measurements of a cartilage section with an initial thickness of 15.2 μm a) first in DI water, and then in b) 1 \times PBS after 12 hours of equilibration in each solution. Three compressions -red diamonds (f1), circles (f2) and triangles (f3)- and decompressions -green diamonds, circles and triangles- are shown in each diagram. The hysteresis between compression and decompression in DI water and the variation of consecutive compressions indicate that structural changes happen, and the cartilage does not recover between consecutive measurements. These results are qualitatively similar to those described in the main manuscript in 1 \times PBS. After the measurements in DI water, the compression was measured in 1 \times PBS after equilibration. Note that the hysteresis and the difference between consecutive compressions in 1 \times PBS (after DI water) are much less prominent. This behavior deviates from the results described in the main manuscript and indicates that the time-dependent change of the microstructure is much less prominent after the first set of compression isotherms (independently of the fluid, DI water or 1 \times PBS). In other words, the compression is the origin for the changes of the microstructure, and not the ionic strength (DI water vs. 1 \times PBS).

The adhesion of cartilage to mica in eSFA experiments was negligible under all conditions, including in the presence of calcium. This is not surprising since calcium ions only bind to mica at concentrations greater than 100 mM (1), which were not examined here.

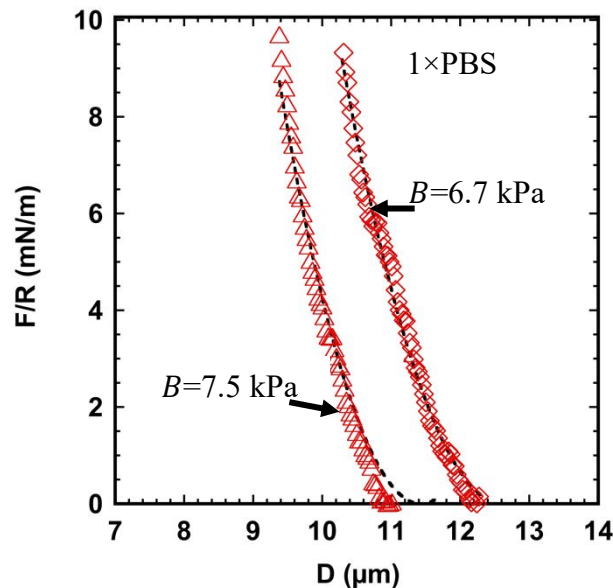


Figure S2. Representative fits of the compressibility model (Eqn. (1) in the main manuscript) to measured compression isotherms in 1× PBS. This yields compressive moduli (B) of 6.7 and 7.5 kPa, respectively. The fit is only possible for the first 1-1.5 μm , indicating that the compressive modulus changes (increases) with depth. This is consistent with the nanoindentation results.

ATR-IR spectroscopy

Figure S3 shows representative results for the cartilage sections. The IR absorbance reveals the presence of a) amide I (1632 cm^{-1}) and amide II (1553 cm^{-1}), b) the sulfate stretch (1240 cm^{-1}), and c) the carbohydrate region ($970\text{-}1180\text{ cm}^{-1}$) in all cartilage sections (bottom and top interfaces). Interestingly, the flat peak of amide I shown in all measurements of the “bottom” interface is similar to that of aggrecan (2). This is not observed in the measurements of the “top” regions, indicating that this region is less rich in proteoglycans. This is further supported by the smaller absorbance of the carbohydrate region in all measurements of the “top” interface.

A previous work has reported the IR spectra of collagen (mainly type I) and elastin from the aorta and combinations of them at different mass ratios (3). Although the spectra of elastin and collagen are very similar due to their protein content, a distinction was possible in that work. For example, the absorbance of amide I in elastin is in the range $1610\text{-}1645\text{ cm}^{-1}$, whereas it is $1643\text{-}1667\text{ cm}^{-1}$ for collagen; other works report $\sim 1655\text{ cm}^{-1}$ for collagen type II in bovine cartilage (2). In our measurements, the absorbance of amide I lies in the range $1632\text{-}1652\text{ cm}^{-1}$, and hence, it is possible that there is an enrichment of elastin fibers in the cartilage sections. Collagen and elastin have also some distinct features in the range $1420\text{ - }1300\text{ cm}^{-1}$, like the more pronounced peaks at 1404 , 1378 and 1319 cm^{-1} of elastin, also observed in Figure S3. While the reported spectra in ref. (2) do not correspond to elastin from cartilage, and hence, they need to be considered cautiously, they suggest that we cannot exclude the presence of elastin in the investigated cartilage sections.

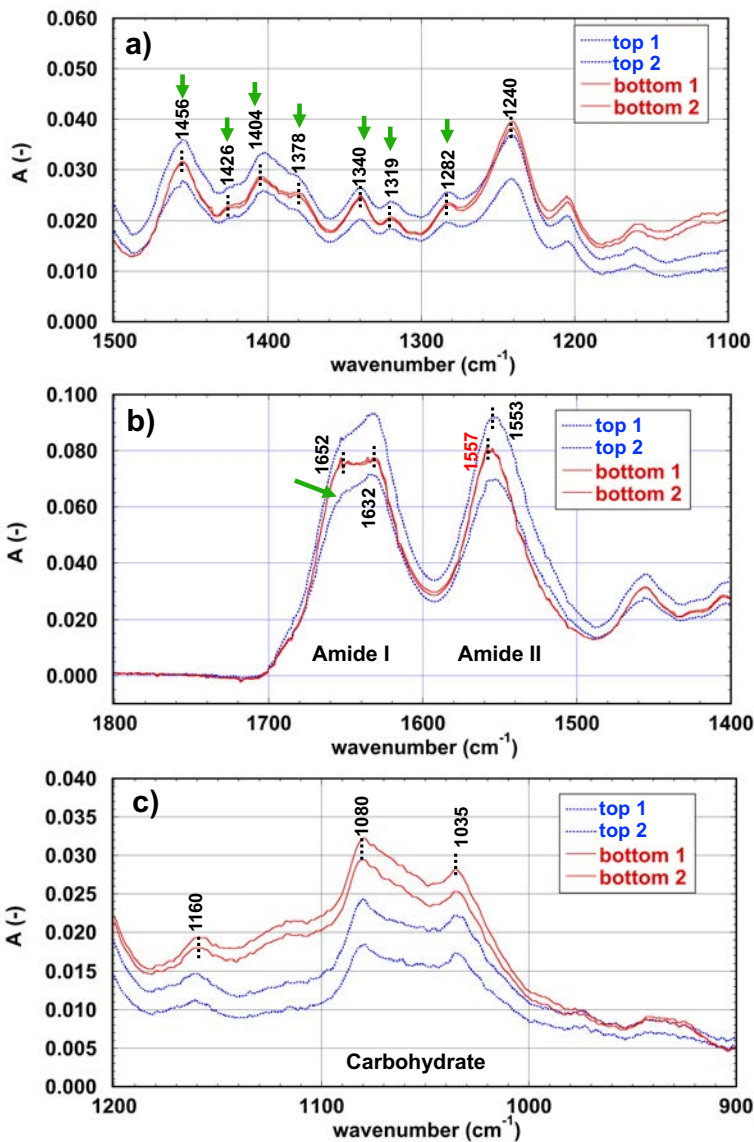


Figure S3. Representative ATR-IR spectra of hydrated cartilage sections after subtraction of the baseline of water. The penetration depth of the IR beam is 1 to 2 μm in the top and bottom interfacial regions. The labels “top” and “bottom” indicate that upper and bottom regions are in contact with the ATR crystal, respectively, and therefore, they are probed.

AFM nanoindentation

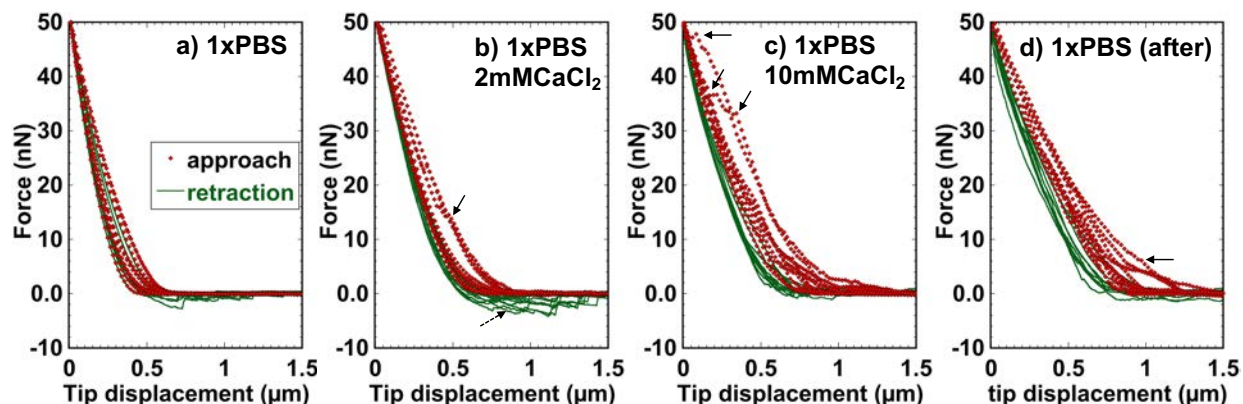


Figure S4. Representative indentation force vs. depth curves measured by colloidal probe AFM in areas of $10\ \mu\text{m} \times 10\ \mu\text{m}$ in (a) $1\times$ PBS with no calcium, b) with $1.8\ \text{mM}$ CaCl_2 , c) with $10\ \text{mM}$ CaCl_2 and d) re-equilibration in $1\times$ PBS with no calcium (denoted “after”). Extension (red full diamonds) and retraction (green lines) curves are shown in each plot. The irregularities in the approach curves (see arrows) indicate that the tip snaps into the cartilage due to an attractive force, which is associated with the ionic bridging mediated by the calcium ions. Even in $1\times$ PBS (after), snap-in events are observed, which implies that the calcium ions are still bound to the cartilage, and hence, the storage overnight in $1\times$ PBS did not remove the ions. Colloid radius: $10\ \mu\text{m}$, Cantilever stiffness: $0.45\ \text{N/m}$.

Note that the adhesive force is negligible except upon addition of $1.8\ \text{mM}$ CaCl_2 (b), although it is still small. Adhesion can be justified by the calcium mediated bridging between the negatively charged molecules in the cartilage surface and the silanol groups at the silica surface. Interestingly, the adhesion between the cartilage and the colloid vanishes in $10\ \text{mM}$ CaCl_2 solution. The origin for this surprising behavior could be related to the saturation of the negative sites of both the cartilage and the probe at this high concentration, which leads to an overall electrostatic repulsion between the two “positively” charged surfaces; a phenomenon known by the colloid community as charge reversal (4). In fact, it is known that charge reversal of silica happens at concentrations between 1 and $10\ \text{mM}$ (5), and hence, it is possible here. The adhesion remains low under re-equilibration of the cartilage in $1\times$ PBS in the absence of calcium, which suggests that calcium binding is irreversible within the duration of this experiment.

Note that the stick-slip observed in friction-force measurements is related to the ionic bridging between silica and cartilage provided by calcium, which seems to be a contradiction with the results shown in Figure S4. However, a major difference between indentation and static-friction force measurements is the loading time; during pull-off force measurements, the loading time is smaller than $1\ \text{s}$, whereas in static friction-force measurements, the loading time is greater than $5\ \text{s}$. This suggests that calcium bridging at the interface and the associated stick-slip requires sufficient dehydration of the cartilage.

Hertz model

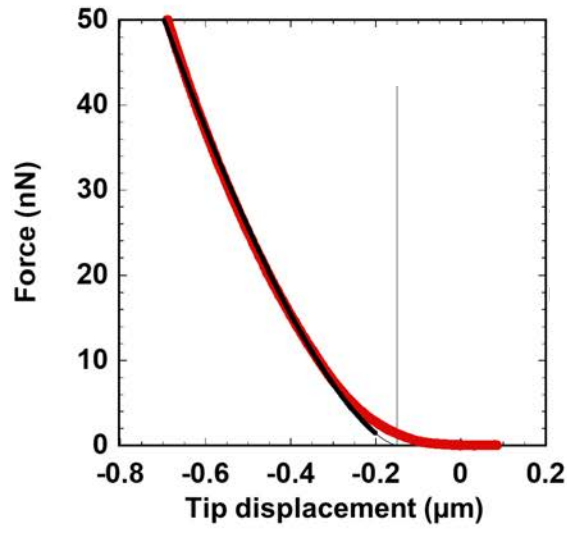


Figure S5. Representative indentation force vs. depth curve measured on the cartilage's articulating surface in equilibrium with 1× PBS (red) and Hertzian fit to the experimental data (black line). At loads smaller than ~5 nN, there is a clear deviation from the model, and hence, the Hertz model is applied piecewise as described in the materials and methods section. Colloid radius: 10 μm , Cantilever stiffness: 0.45 N/m.

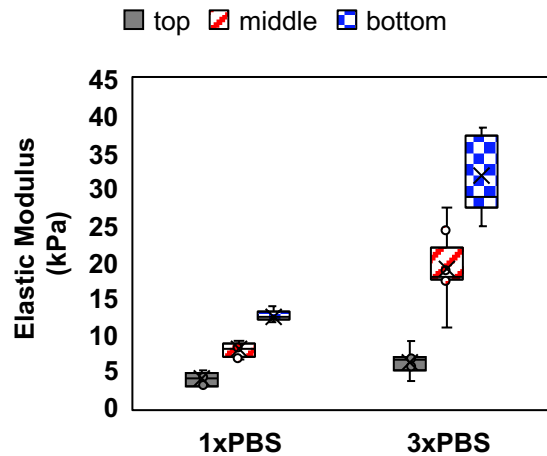


Figure S6. Elastic modulus according to the Hertz model in 1× PBS and 3× PBS. The Hertz model was applied “piecewise” to determine top, middle and bottom moduli. The increase of the elastic modulus in 3xPBS is observed in the three regions, and it can result from the contraction of the cartilage to balance the osmotic pressure.

Table S1. Calculation of the saturation index (SI_x) of minerals in 1xPBS and 1.8mM CaCl₂. The minerals that can precipitate are given in red.

Mineral	log IAP	SI_x=log IAP- log K_s
Aragonite	-10.231	-1.895
Ca ₃ (PO ₄) ₂ (am1)	-25.763	-0.263
Ca ₃ (PO ₄) ₂ (am2)	-25.763	2.487
Ca ₃ (PO ₄) ₂ (beta)	-25.763	3.157
Ca ₄ H(PO ₄) ₃ :3H ₂ O(s)	-44.322	3.628
CaCO ₃ xH ₂ O(s)	-10.233	-17.859
CaHPO ₄ (s)	-18.552	0.723
CaHPO ₄ :2H ₂ O(s)	-18.556	0.438
Calcite	-10.231	-1.751
Halite	-1.939	-3.489
Hydroxyapatite	-32.976	11.357
KCl(s)	-3.507	-4.407
Lime	11.338	-21.361
Natron	-8.807	-7.496
Portlandite	11.336	-11.368
Thermonatrite	-8.786	-9.423
Vaterite	-10.231	-2.317

Table S2. Calculation of the saturation index (SI_x) of minerals in 1xPBS and 10mM CaCl₂.

Mineral	log IAP	SI_x=log IAP- log K_s
Aragonite	-9.635	-1.299
Ca ₃ (PO ₄) ₂ (am1)	-23.837	1.663
Ca ₃ (PO ₄) ₂ (am2)	-23.837	4.413
Ca ₃ (PO ₄) ₂ (beta)	-23.837	5.083
Ca ₄ H(PO ₄) ₃ :3H ₂ O(s)	-41.732	6.218
CaCO ₃ xH ₂ O(s)	-9.638	-17.263
CaHPO ₄ (s)	-17.887	1.388
CaHPO ₄ :2H ₂ O(s)	-17.892	1.103
Calcite	-9.635	-1.155
Halite	-1.9	-3.45
Hydroxyapatite	-29.79	14.543
KCl(s)	-3.468	-4.368
Lime	11.934	-20.765
Natron	-8.966	-7.655
Portlandite	11.932	-10.772
Thermonatrite	-8.942	-9.579
Vaterite	-9.635	-1.721

Table S3. Loading conditions in AFM and eSFA experiments. Contact pressure and radius in indentation measurements were calculated based on the Hertz model. The contact radius in eSFA experiments was obtained geometrically as $a = R \cdot \sin \theta$, with $\cos \theta = 1 - \delta/R$, and the maximum contact pressure as the ratio between maximum load (3 mN) and contact area πa^2 . The time scale of the compression was estimated as the maximum deformation divided by the velocity $V = 1 \text{ nm/s}$.

	Nanoindentation (AFM)	Slow compression (eSFA)
Tip radius	10 μm	2 cm
Maximum load	50 nN	3 mN
Approach velocity (V)	0.8 $\mu\text{m/s}$	1 nm/s
Max. deformation (δ)	$\sim 1 \mu\text{m}$	$\sim 6 \mu\text{m}$
Max. contact pressure	$\sim 10 \text{ kPa}$	$\sim 6 \text{ kPa}$
Max. contact radius	$\sim 3 \mu\text{m}$	$\sim 500 \mu\text{m}$
time scale compression	$< 1.5 \text{ s}$	$< 2 \text{ h}$

References

1. Alcantar N, Israelachvili J, & Boles J (2003) Forces and ionic transport between mica surfaces: implications for pressure solution. *Geochim Cosmochim Acta* 67(7):1289-1304.
2. Camacho NP, West P, Torzilli PA, & Mendelsohn R (2001) FTIR microscopic imaging of collagen and proteoglycan in bovine cartilage. *Biopolymers* 62(1):1-8.
3. Cheheltani R, *et al.* (2014) Fourier transform infrared spectroscopy to quantify collagen and elastin in an in vitro model of extracellular matrix degradation in aorta. *Analyst* 139(12):3039-3047.
4. Israelachvili JN (2011) *Intermolecular and surface forces* (Academic press) 3rd Ed.
5. Diao Y & Espinosa-Marzal RM (2016) Molecular insight into the nanoconfined calcite-solution interface.